Studying angularly extended gamma-ray sources with VERITAS

Research Thesis

Presented in partial fulfillment of the requirements for graduation

with research distinction in Astronomy & Astrophysics

in the undergraduate colleges of The Ohio State University

by

Gabriela Torrini

The Ohio State University

April 2020

Abstract

The Very Energetic Radiation Imaging Telescope Array System (VERITAS) observes astronomical sources emitting γ-rays in the energy range from 85 GeV to 30 TeV. VERITAS can detect a point-like source with 1% of the Crab Nebula flux in a 25-hour long exposure. During the past decade, VERITAS has observed the Geminga supernova remnant for 93 hours. Although Geminga has 23% of the Crab Nebula flux, it has not been successfully imaged yet due to its large spatial extent. Telescopes from the Milagro Experiment have detected Geminga with an angular diameter of 2.6°, which occupies over 5 times more space in the sky than the moon (Abdo et al. 2009). Currently, two standard methods are used to subtract the cosmic ray background from images of a γ-ray source. To estimate the background, these methods compare the source to surrounding areas within the telescope's field of view (FOV). However, these methods do not work for spatially extended sources like Geminga, where the region of interest (ROI) is comparable in size to the FOV. The Matched Run Method (MRM) was developed to allow for comparison between the ROI and other regions of the sky. The MRM algorithm estimates the background by matching observations from different sources with similar characteristics. I optimized the algorithm by studying how parameters such as γ-ray shower shape, elevation, azimuth, and season affected the success of matches. The improved version of the MRM will enable VERITAS to accurately image spatially extended sources.

Acknowledgements

I want to thank:

- My thesis committee members, Dr. Laura Lopez & Dr. Don Terndrup,
- My REU advisors, Dr. Udara Abeysekara & Dr. Dave Kieda,
- The National Science Foundation (Award # 1659494), the U.S. Department of Energy, the Smithsonian Institution, the Natural Science & Engineering Research Council in Canada, the Science & Technology Facilities Council in the UK, and Science Foundation Ireland, and
- The VERITAS Collaboration.

Contents

List of Figures

List of Tables

Acronyms

AGN active galactic nuclei.

CFD constant fraction discriminator.

EAS extensive air shower.

FADC flash analog-to-digital converter.

FOV field of view.

HAWC High Altitude Water Cherenkov.

IACT Imaging Atmospheric Cherenkov Telesope.

ISM interstellar medium.

LAT Large Area Telescope.

MJD modified Julian date.

MRM Matched Run Method.

MSCW mean scaled width.

NCR number of cosmic-ray events.

NSB Night sky background.

PMTs photomultiplier tubes.

PWNe pulsar wind nebulae.

RBM ring background method.

ROI region of interest.

SAS-2 Small Astronomy Satellite 2.

SNRs supernova remnants.

VERITAS Very Energetic Radiation Imaging Telescope Array System.

VHE very high energy.

Chapter 1

INTRODUCTION

1.1 What are γ-rays?

For most of history, humanity's knowledge of the cosmos relied on observations of optical light. Eyes, mirrors, and lenses helped decode the motions of planets and stars. After World War II, technological advances made radio and X-ray astronomy possible. However, the most energetic portion of the electromagnetic spectrum was not explored until the 1960s (Weekes 2003).

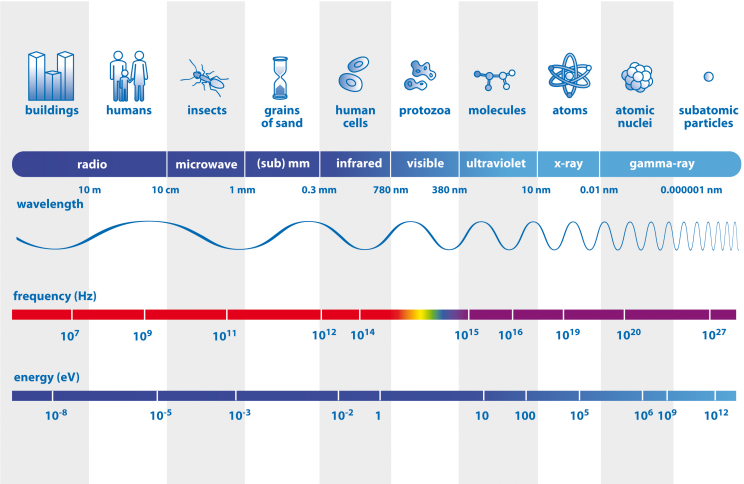

Figure 1.1: The electromagnetic spectrum.[†]

[†]Image from www.solar-center.stanford.edu/about/uvlight.html.

γ-ray photons possess the highest frequencies (and consequently, highest energies) of any electromagnetic radiation (see Figure 1.1). Their incredibly short wavelengths prevent them

from being effectively reflected by mirrors. Coupled with their inability to penetrate Earth's atmosphere, this issue delayed the detection of cosmic γ-rays.

The first cosmic γ-ray observations occurred with the assistance of satellites. Using dense, crystal lattice detectors, these satellites observed γ-ray emission from point sources like pulsars and X-ray binaries within the Milky Way. The unintentional discovery of γ-ray bursts from the Vela satellites in the late 1960s sparked major investment in the field of γ-ray astronomy (Weekes 2003). By 1991, NASA launched its first dedicated γ-ray mission, the Compton Gamma-Ray Observatory (Di Sciascio 2019).

Despite the success of space-based detection, it was costly to build and maintain γ-ray observatories. The construction bounds on detector sizes limited observations. Since these observatories did not use mirrors, the effective aperture of the γ-ray 'telescope' was determined by the size of the detector (Weekes 2003). In addition, the typical flux of cosmic γ-ray sources is incredibly weak, so statistically significant observations required long exposures. For example, space telescopes have detected a faint flux of one photon per minute from the Vela Pulsar, which is the strongest γ-ray source at 100 MeV energies (Weekes 2003).

1.2 Ground-based detection

In 1934, the Italian physicist Bruno Rossi discovered the production of an extensive air shower (EAS), a cascade of charged particles, while studying cosmic rays[1]. Cosmic rays are massive, high-energy particles originating in space.

During the 20th century, particle physics experiments predicted that very high energy (VHE) TeV γ-rays could be emitted through various interactions (see Section 1.4). If such γ-rays interacted with particles at the top of the atmosphere, they could impart tremendous energy and momentum, initiating an EAS. In the late 1960s, the Italian physicist Giuseppe Cocconi suggested to search for cosmic γ-ray sources via air showers (Di Sciascio 2019).

At the start of an EAS, a γ-ray interacts with an atmospheric nucleus. This initiates pair production, in which a relativistic electron and positron sharing the energy of the original γ-ray move downward symmetrically. After travelling a radiation length, these particles will slow down and release lower energy photons via bremsstrahlung, which can then cause further pair production. As the cascade progresses, the number of particles increases while the energies of individual particles decreases.

[1] "A History of Gamma-Ray Astronomy Including Related Discoveries", 2009. www.heasarc.gsfc.nasa.gov/docs/history/

The atmosphere contains a mixture of molecules and is not a vacuum-like environment. Under standard atmospheric temperature and pressure conditions, light travels at a factor of 1/1.000293 times its speed in a vacuum, or 298,916,632 m/s [1]. When relativistic particles in the cascade have a higher velocity than the phase velocity of the slowed-down light, a shock wave occurs, emitting a cone of Cherenkov radiation.

Cherenkov radiation can be detected optically. It produces the characteristic blue glow seen in underwater nuclear reactors. The size of the cone of Cherenkov light depends on particle speed: the faster the particles, the smaller the opening angle of the cone.

An EAS begins high up in the atmosphere, at about 20 kilometers above the surface of the Earth. Most γ-ray air showers produce a Cherenkov cone with an opening angle of about 1°, which spreads into a light pool with an approximate radius of 130 meters on the ground. Cherenkov flashes typically last a few nanoseconds. From the ground, the weak cosmic γ-ray flux can be detected over much larger areas than available for space-based detectors. Far down from the small Cherenkov cone, ground-based telescopes could pose a huge advantage. In fact, the effective collecting area from the ground is equivalent to the shower front area, not the geometrical area of the detector.

In 1989, the Whipple Observatory witnessed the first solid detection of TeV cosmic γ-rays coming from the Crab Nebula (Di Sciascio 2019). Using a 10-meter reflector, the Whipple Observatory revolutionized the detection of cosmic γ-rays via the Imaging Atmospheric Cherenkov Telesope (IACT).

1.3 VERITAS

The Very Energetic Radiation Imaging Telescope Array System (VERITAS) is a modern IACT housed at the Whipple Observatory in Arizona. Whereas the first IACTs only consisted of one telescope, VERITAS is an array of four 12-meter telescopes (see Figure 1.2). Each telescope contains a mount, an optical system, and a camera. The telescopes are pointed in a source direction by the steerable mount, which controls elevation and azimuth. Cherenkov light is collected by the reflector, which consists of 350 hexagonal mirrors with over 90% reflectivity (*ACT Techniques & VERITAS Technology* 2011). Once reflected, this light travels to a camera at the telescope's focal plane. The 499-pixel camera has the same number of photomultiplier tubes (PMTs) and provides a 3.5° field of view (*ACT Techniques & VERITAS Technology* 2011).

[1] Hecht, Eugene (2002). *Optics*. Addison-Wesley.

Figure 1.2: The four telescopes used by VERITAS.†

†Image from the VERITAS Collaboration

VERITAS is sensitive to sources emitting γ-rays within the energy range of 85 GeV to 30 TeV and has one of the highest detection ranges of any active IACT (see Table 1.1). Besides its merit as an IACT, VERITAS has observational and logistical advantages over lower energy threshold space-based telescopes and higher energy threshold water Cherenkov telescopes. The Fermi Large Area Telescope (LAT) only has an effective collection area of about 0.65 m^2, while VERITAS can collect over an area of about 100,000 m^2 (Funk 2015). Since water Cherenkov telescopes require the Cherenkov radiation to occur at the detector site, they must operate at higher altitudes where air showers are more likely to penetrate all the way to the ground. IACTs like VERITAS simply detect Cherenkov radiation that propagates down from the atmosphere. For example, the High Altitude Water Cherenkov (HAWC) Observatory resides at 4100 meters, while VERITAS operates at 1268 meters (Funk 2015). For the very high energy (VHE) range of γ-rays, VERITAS is an ideal observatory. However, it is limited to observing during dark nights. Other types of γ-ray telescopes can observe at any time of day.

IACT	VERITAS†	HESS*	MAGIC‡	CTA⋆
Energy Range (GeV)	85-30,000	30-100	25-50	20-300,000
Diameter (m)	12	15 & 36	17	8, 12, & 23
# Telescopes	4	5	2	120
Field of View (°)	3.5	5.0 & 3.2	3.6	4.3-10.5

Table 1.1: VERITAS compared to current (HESS, MAGIC) and future (CTA) IACTs.

†www.veritas.sao.arizona.edu/about-veritas-mainmenu-81/veritas-specifications-mainmenu-111
*www.mpi-hd.mpg.de/hfm/HESS/pages/about/HESS_I_II/
‡www.mpp.mpg.de/en/research/astroparticle-physics-and-cosmology/magic-and-cta-gamma-ray-telescopes/magic/
⋆www.cta-observatory.org/project/technology/

1.4 Emission mechanisms & sources

Cosmic γ-rays produce emission through 4 processes: inverse Compton scattering, synchrotron, brehmsstrahlung, and neutral pion decay (see Figure 1.3). Inverse Compton scattering occurs due to the collision of a relativistic electron and a low-energy photon and is found in pulsar wind nebulae (PWNe) and active galactic nuclei (AGN). Synchrotron radiation occurs when a relativistic electron in the presence of a strong magnetic field moves in a helical path along the line of magnetic force, and it is dominant in PWNe. Brehmsstrahlung occurs when a relativistic electron is deflected by the electric field of an atomic nucleus or molecule. Dense, gaseous material in supernova remnants (SNRs) and the interstellar medium (ISM) are ideal environments for brehmsstrahlung with cosmic electrons. γ-rays produced by neutral pion decay occurs in SNRs.

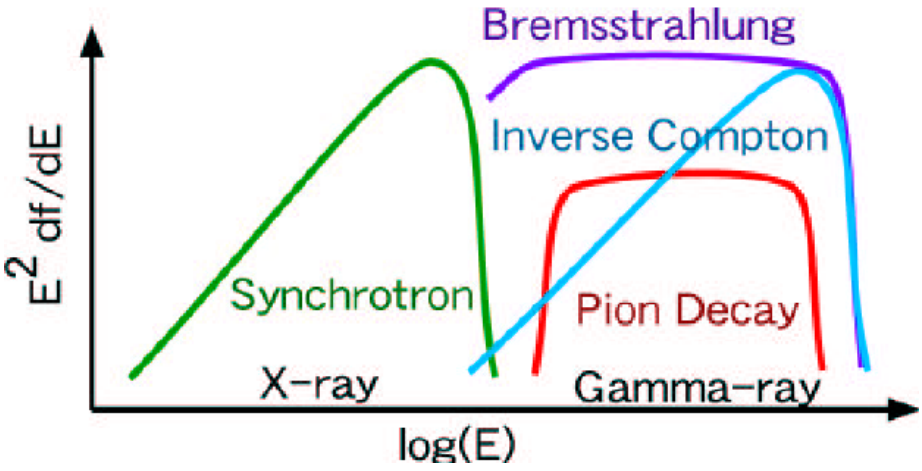

Figure 1.3: Schematic diagram of various emission mechanisms and their energy domains.†

†Image from T. Tanimori, in *Proceedings of the 31st SLAC Summer Institute on Particle Physics, Stanford, 2003*, edited by J. Hewett, J. Jaros, T. Kamae, C. Prescott, eConf C0307282, TTHO7 (2003).

Chapter 2

BACKGROUND & DETECTION

2.1 Background radiation

2.1.1 Cosmic rays

Similar to a primary γ-ray, cosmic rays produce their own extended air showers and subsequent Cherenkov light (see Figure 2.1). The primary source of hadronic showers is protons (hydrogen nuclei), though heavier nuclei, electrons, and positrons can also produce these showers. In the VHE domain, the number of cosmic-ray background events is about 1000–10,000 times the number of generic γ-ray radiation events (Weekes 2003). The higher distribution of cosmic rays made it nearly impossible for early IACTs to differentiate between electromagnetic and hadronic air showers. With the help of more telescopes and stereo

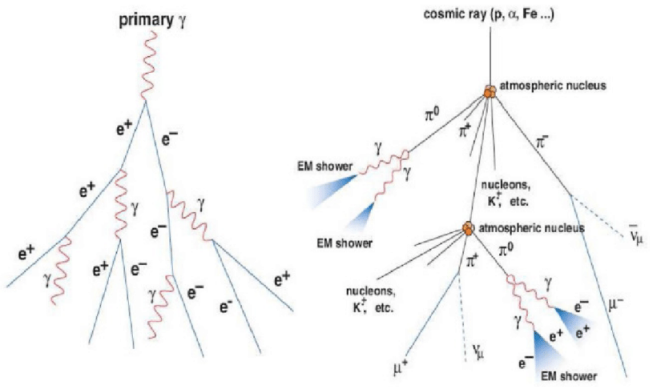

Figure 2.1: γ-ray air shower (*left*) versus a cosmic ray air shower (*right*).[†]

[†]Image from Lopez Oramas, A. 2014, "Multi-year campaign of the gamma-ray binary LS I +61°303 and search for VHE emission from gamma-ray binary candidates with the MAGIC telescopes".

detection, modern IACT arrays have started filtering out the cosmic ray background.

In 1985, the British physicist Michael Hillas proposed a set of features, called Hillas parameters, that could be used to distinguish between electromagnetic and hadronic showers (Hillas 1985). When either type of shower is detected, it appears as an elliptical pixel image contour in the camera, yielding a unique angular distribution. Hillas classified shape and orientation parameters: width and length, and α and distance, respectively. The parameters are defined as such (see Figure 2.2):

- **Width**: The root mean squared spread of light along the minor axis of the ellipse. Provides information about the *lateral* development of the shower.
- **Length**: The root mean squared spread of light along the major axis of the ellipse. Provides information about the *longitudinal* development of the shower.
- $\boldsymbol{\alpha}$: The angle between the major axis of the ellipse and the line drawn from the center of the camera (the source position) to the centroid.
- **Distance**: The separation between the center of the camera (the source position) and the centroid.

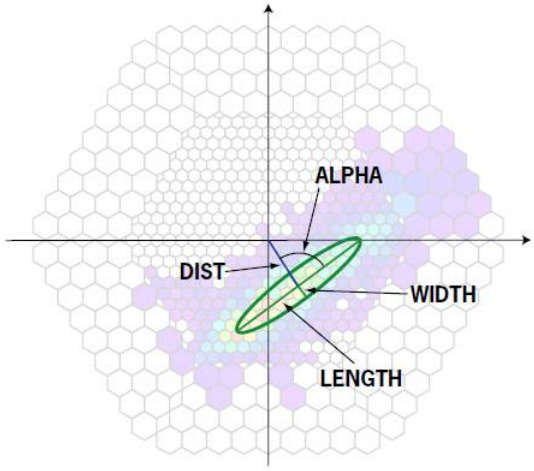

Figure 2.2: The Hillas parameters for distinguishing between air shower sources.†

†Image from ETH Institute of Particle Physics.

γ-ray air showers tend to have smaller width and α values. The secondary emission in a γ-ray cascade is more symmetric, so the lateral spread in Cherenkov light is not as large. When observing a specific γ-ray source, the major axis of the ellipse will be more parallel

to the telescope axis. Conversely, cosmic ray air showers tend to have larger width and α values. The secondary particles from a cosmic ray interaction are emitted at wider angles. Assuming a fairly isotropic cosmic-ray background, the major axis of the ellipse can then point in any direction.

2.1.2 Sky brightness & local muons

Another background source is the visible light near observatories. From the night sky, sources include airglow, meteors, stars, and lightning. In fact, the Cherenkov radiation from an EAS is so faint that VERITAS does not observe during full moons. From humans, sources include airplanes, city lights, and satellites. Since Cherenkov flashes are on the order of a few nanoseconds, variable sources of light affect observations more than steady ones.

Relativistic muons that are close to the telescopes will generate cones of Cherenkov light that appear as short arcs in the camera, similar to a γ-ray pixel contour. Fortunately, these local muons tend to have small enough Cherenkov cones that they are only detected by a single telescope, not the entire array (J. Holder et al. 2006).

2.1.3 Detection

In order to distinguish between a γ-ray signal and the various background sources, VERITAS has a 3-level trigger system in place:

- **Pixel Trigger**: Each PMT pixel in the camera is paired with a constant fraction discriminator (CFD). The output of the PMT is relayed to the input of the CFD. Then, the CFD produces an output logic pulse if the sum of voltages from the PMT pulse and a time-delayed copy cross a predetermined threshold. The current threshold implemented by VERITAS is 50 mV, or about 4 to 5 photoelectrons (Weinstein 2008).

- **Pattern Trigger**: Night sky background (NSB) fluctuations can easily cause the level one trigger, especially if the CFD threshold is low. To allow for a lower CFD threshold while rejecting background signals, another trigger is implemented. To initiate the level two trigger, several adjacent pixels must cross the CFD threshold within about 6 ns (Weinstein 2008).

- **Array Trigger**: If a pattern triggers occur on multiple telescopes, the level three trigger initiates data acquisition. Checking for coincidence on multiple telescopes makes

rejection of local muon signals possible and enables the CFD threshold to be lowered even more to a regime where muons would have dominated.

2.2 Geminga

An unidentified γ-ray point source was first detected by NASA's Small Astronomy Satellite 2 (SAS-2) in 1973 and subsequently confirmed by the ESA satellite COS-B (Weekes 2003). The source was radio-quiet and possessed a low γ-ray-to-radio intensity. Since this feature was also present in the Vela and Crab pulsars, the search for a periodic signal began across various wavelengths. In 1992, the German X-ray satellite ROSAT detected pulsations from the source (Halpern and Holt 1992). After almost 20 years, the point source was finally identified as a pulsar.

Since the 1990s, observations have measured a larger fraction of multi-GeV cosmic positrons than predicted by theoretical models (Moskalenko and Strong 1998). When travelling towards Earth from great distances, high-energy positrons can rapidly lose energy. To explain this observed excess, particle physicists began searching for local sources of high-energy, charged cosmic radiation.

VHE γ-rays are often produced by pulsar-driven winds, as demonstrated by the Vela and Crab pulsars. Geminga is 250 pc away, and its radio-quiet pulsar is contained within a larger SNR. Geminga could explain more than just the cosmic positron excess. It has also been posited as a cause of the Local Bubble, a nearby, hot, low-density void (Gehrels and Chen 1993).

During the past decade, VERITAS has observed the Geminga SNR for over 93 hours. VERITAS can detect a point-like source with 1% of the Crab Nebula flux in a 25-hour long exposure. Although Geminga has 23% of the Crab Nebula flux, it has not yet been successfully imaged by VERITAS. The established methods for point-source analysis are not compatible with angularly extended sources, as VERITAS cameras only have a 3.5° field of view (FOV). The HAWC Observatory and the Milagro Experiment have detected Geminga with extensions of 2° and 2.6°, respectively (Abeysekara et al. 2017, Abdo et al. 2009). Based on the latter observation, Geminga could occupy over 5 times more space in the sky than the moon.

2.3 Current methods

Selective cuts based off of the Hillas parameters can reduce the cosmic-ray background by a factor of about 100 (Berge, Funk, and Hinton 2007). However, the significance of γ-ray signals cannot be determined without knowing the number of γ-ray-like events. The γ-ray excess is given by

$$N_{\text{excess}} = N_{\text{ON}} - \alpha N_{\text{OFF}} \tag{2.1}$$

where N_{ON} is the number of counts in the source region, N_{OFF} is the number of counts in the background region, and α is the ratio of the source region area to the background region area (Flinders 2015). The values for α and N_{OFF} come from cosmic-ray background estimation techniques. VERITAS has used two such methods: the ring background method (RBM) and the reflected region method.

The RBM estimates the background from a ring around the source region. The reflected region model estimates the background from a set of regions equally offset from the source position. Each off region in the reflected region model shares the same size and shape as the source region. Sources with larger angular sizes require larger background estimation areas (a larger ring or more offset regions). But for sufficiently extended sources, the amount of background regions contained within the FOV is limited by an overlapping region of interest.

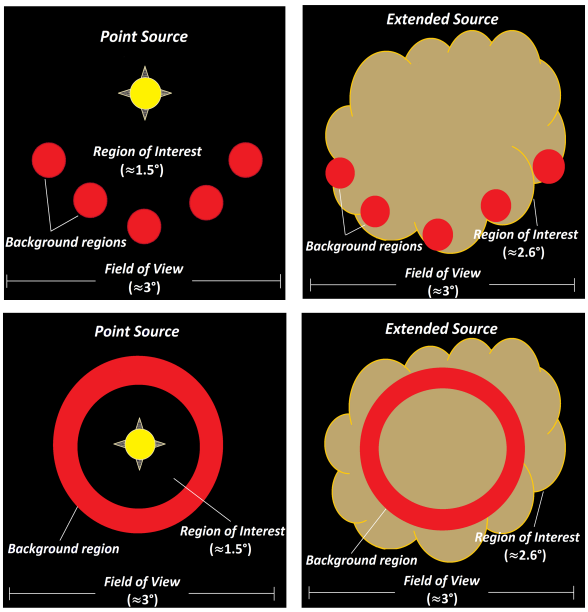

Figure 2.3: The reflected region method (*top panels*) versus the RBM (*bottom panels*).

Greater α values mean higher uncertainties, both in the background estimation and in the final significance of the observation. With the FOV-limited RBM and reflected region method, obtaining satisfactory α values for extended sources is not possible (see Figure 2.3).

2.4 The Matched Run Method

One method proposed for analyzing extended sources is the Matched Run Method (MRM). The MRM algorithm matches data from a source observation (*ON* run) with data from a secondary FOV (*OFF* run). The OFF run should have a comparable background rate and similar hardware configurations to the ON run. A variety of conditions could yield suitable OFF runs for background matching:

- The OFF run follows the same elevation and azimuth path as the ON run, and is taken immediately before/after the source observation.
- The OFF run is in a distinct FOV with no trace of γ-ray emission.

Lists of ON and OFF runs are inputted into the algorithm. Then, the algorithm matches pairs of runs that satisfy predefined tolerances for deviation in elevation angle, azimuthal angle, and observation date. I optimized the algorithm by analyzing the impact of these various observing parameters on predicted match success.

Chapter 3

METHODS

3.1 Overview

In order to accurately count the number of cosmic-ray events (NCR), I performed a statistical analysis of different mean scaled width (MSCW) ranges. After determining the appropriate range to use for hadron counting, I changed the calibration for the standard analysis pipeline, EVENTDISPLAY.

Next, I created a Python script to predict which tolerances for deviation in elevation angle, azimuthal angle, and observation date would yield the greatest match success. These tolerances were then implemented in the MRM algorithm.

I analyzed over 100 hours of data from 3 sources using EVENTDISPLAY and the MRM algorithm:

- Segue 1, a dwarf spheroidal galaxy
- 1ES 0229+200, a BL Lacertae object
- Markarian 421, a blazar

The MRM results were compared to standard analysis output for validation.

3.2 Cosmic Ray Counting Analysis

In summer 2012, the VERITAS cameras were upgraded with high-quantum-efficiency PMTs. As a consequence, the established MSCW ranges used for filtering between γ-rays and hadrons in previously collected data were not appropriate for counting NCR in newer data.

I analyzed a 4-hour exposure of the Crab Nebula using eight different MSCW ranges. Using the number of γ-ray like events per run from the EVENTDISPLAY output list file, I calculated the mean, standard deviation, absolute and relative Poissonian errors, and coefficient of variation.

3.3 EVENTDISPLAY Analysis

The EVENTDISPLAY software package analyzes and displays data for ground-based γ-ray observatories. Although it was originally developed for early VERITAS data, EVENTDISPLAY can be modified for various IACT configurations. The software was written in C++ and utilizes data analysis techniques from the library ROOT (Maier and Jamie Holder 2017).

I extracted the number of γ-rays and γ-ray like events from a series of observations using EVENTDISPLAY analysis. After downloading the runlist files from a UCLA database, I processed them with the following analysis tools:

3.3.1 Step 1: evndisp

The noise due to the NSB is estimated from pedestal calculations. Pedestals are voltage offsets in the flash analog-to-digital converter flash analog-to-digital converter (FADC) traces. Next, the charge per pixel and pulse arrival time are integrated from FADC traces. After the signal is extracted, the image is cleaned to further remove contributions from sky brightness fluctuations. If the image pixels and surrounding border pixels are not above a certain predefined threshold, they are removed. Finally, stereoscopic reconstruction tools calculate the origin direction of the γ-ray in the sky and the impact parameter of its respective shower core on the ground.

3.3.2 Step 2: mscw_energy

The γ-ray energies are estimated by Monte Carlo simulations of air showers. Then, the *mscw_energy* tool uses lookup tables to determine the corresponding MSCWs and mean-scaled lengths.

3.3.3 Step 3: anasum

This tool imposes cuts, or boundaries, on the Hillas parameters to select for γ-rays or hadrons. Different cuts are used in certain scenarios:

- **Hard cuts**: The most strict selection level, which almost entirely extracts γ-ray events. Hard cuts are best used for bright sources, when higher rejection of γ-rays is nominal.
- **Moderate cuts**: The intermediate selection level, which mostly extracts events from γ-rays but still allows for some from hadrons.
- **Soft cuts**: The least strict selection level, which extracts a significant amount of events from both γ-rays and hadrons. Soft cuts are best used for dim sources, when lower rejection of γ-rays is necessary.

Also, the *anasum* tool estimates the background via the reflected region method or RBM. These algorithms exclude regions in the FOV containing bright stars or known γ-ray sources.

Once the initial runlist has been processed with these three tools, science analysis can proceed. Using routines from ROOT, I generated skymaps, significance distributions, energy spectra, differential fluxes, and an output list file for each runlist. For each run number, the output list file contains their counts per run, elevation, azimuth, the wobble offset of the telescope during the run, and the modified Julian date (MJD).

3.4 Consistency Analysis

The Consistency Analysis script generates data frames and plots to analyze the difference in observing parameters between ON and OFF runs. I input two list files for the same source: one list file which counts the number of γ-rays and one list file which counts the number of γ-ray-like events or hadrons.

First, the run numbers in each list file are modelled as ON or OFF data in the data frames: the column headers represent ON run numbers, while the row headers represent OFF run numbers. The diagonal entries in the data frame thus share the same ON and OFF run numbers. The data frames display each of the following quantities twice (once for the γ-ray list file and once for the hadron list file):

- OFF-ON count ratio: $\text{Counts}_{\text{OFF}}/\text{Counts}_{\text{ON}}$
- Propagated Poissonian error in OFF-ON count ratio

- Absolute change in azimuth
- Absolute change in elevation
- Absolute change in MJD

Next, the data is classified by consistency. If $|\text{Counts}_{\text{OFF}} - \text{Counts}_{\text{ON}}| \leq (\text{Error}_{\text{ON}} + \text{Error}_{\text{OFF}})$ for both γ-rays and hadrons, then two runs are consistent. This serves as a basic check for predicting match success between runs.

After data is sorted, the variable β is defined:

$$\beta \equiv \frac{\text{Counts}_{\text{OFF, }\gamma\text{-rays}}/\text{Counts}_{\text{ON, }\gamma\text{-rays}}}{\text{Counts}_{\text{OFF, hadrons}}/\text{Counts}_{\text{ON, hadrons}}} \tag{3.1}$$

The distributions of γ-rays and hadrons have characteristic shapes. Despite two runs having distinct curves, the OFF-ON counts ratio should be approximately proportional for γ-rays and hadrons. For an ideal match, $\beta \sim 1$.

Then, the absolute changes in azimuth, elevation, and MJD are plotted against β. This serves as a secondary check for predicting match success between runs.

3.5 MRM Analysis

The MRM algorithm takes two list files as input: a hadron list file including ON runs from the source and a hadron list file including potential OFF runs. The user selects appropriate tolerances for the absolute change in MJD, azimuth, elevation, and NCR between ON and OFF runs. The algorithm matches individual run numbers from each input list by minimizing the difference in observing parameters, especially prioritizing the difference in NCR. The algorithm outputs a .dat file with the pairs once each primary observing run has been matched.

Once the .dat file was produced, I implemented time cuts to make sure that the background was not over- or under-estimated for a given primary observing run. Then I input the .dat file as the runlist for the *anasum* tool to estimate the background. The standard scientific analysis routines (outlined in Section 3.3) were used to generate results.

Chapter 4

RESULTS

4.1 Cosmic Ray Counting Analysis

The V6-epoch of VERITAS began after the PMT upgrade in 2012 and is still ongoing. For V5-epoch VERITAS data, the calibration file used a MSCW range of 0.5-1.5 for counting NCR with hard, 3-telescope cuts. Although no γ-ray bleed-over occurs in the 1.0-1.5 range, Figure 4.1 shows that γ-rays can be detected in the 0.5-1.0 range, even with a short exposure. This hotspot emanating from the Crab Nebula's location is not due to random fluctuations. Figure 4.2 shows the source is detected with $\approx 7\sigma$ significance in the 0.5-1.5 range.

The other 7 MSCW ranges did not display significant detections in their skymaps or significance distributions (see Figure 4.1 and Figure 4.2). I found that 1.0-2.5 was the optimal range for counting NCR, with the highest mean number of counts per run and the smallest relative error (see Table 4.1).

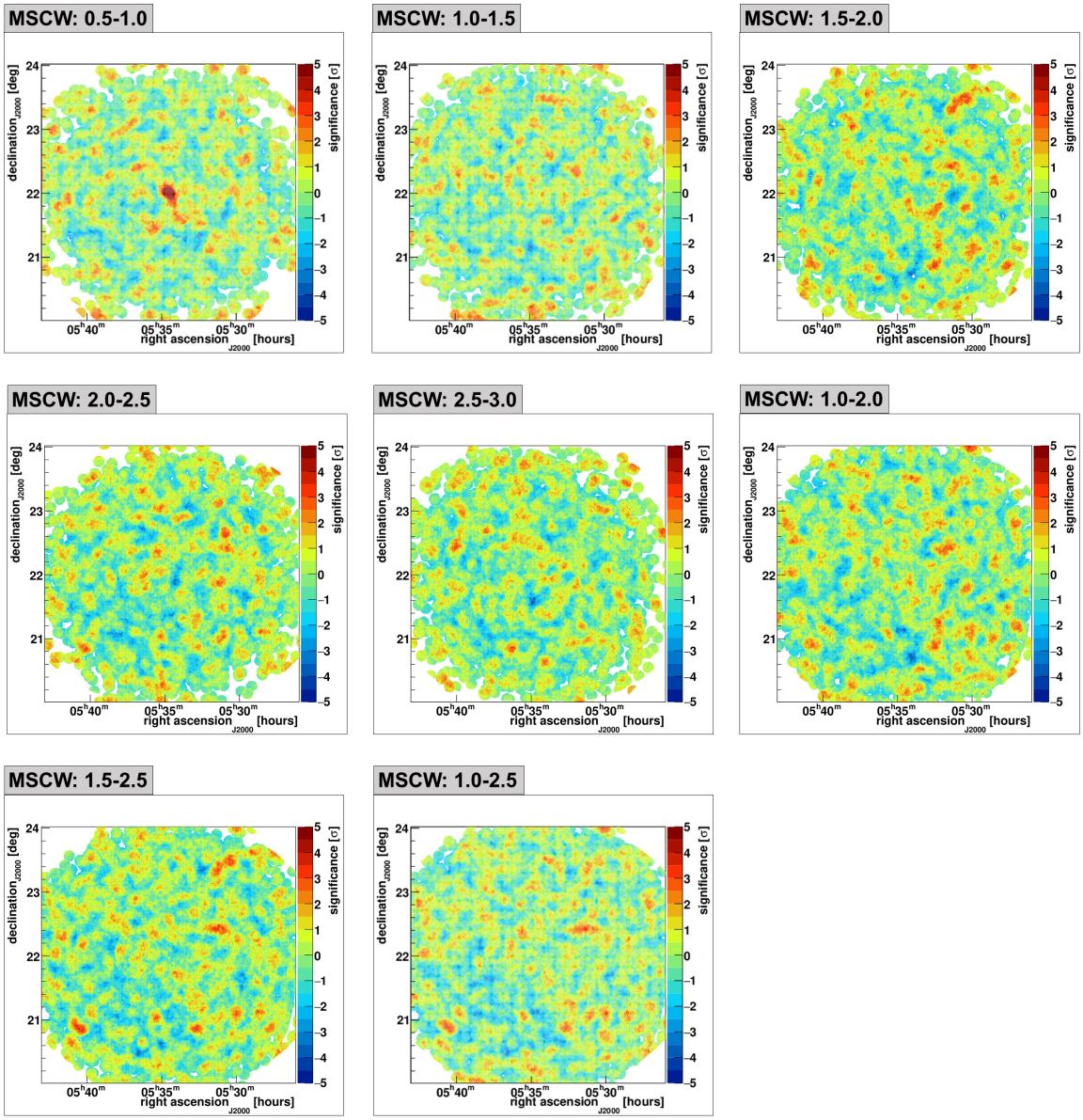

Figure 4.1: Skymaps from a 4-hour exposure of the Crab Nebula. The exposure was analyzed with 8 potential MSCW regions for hadron counting.

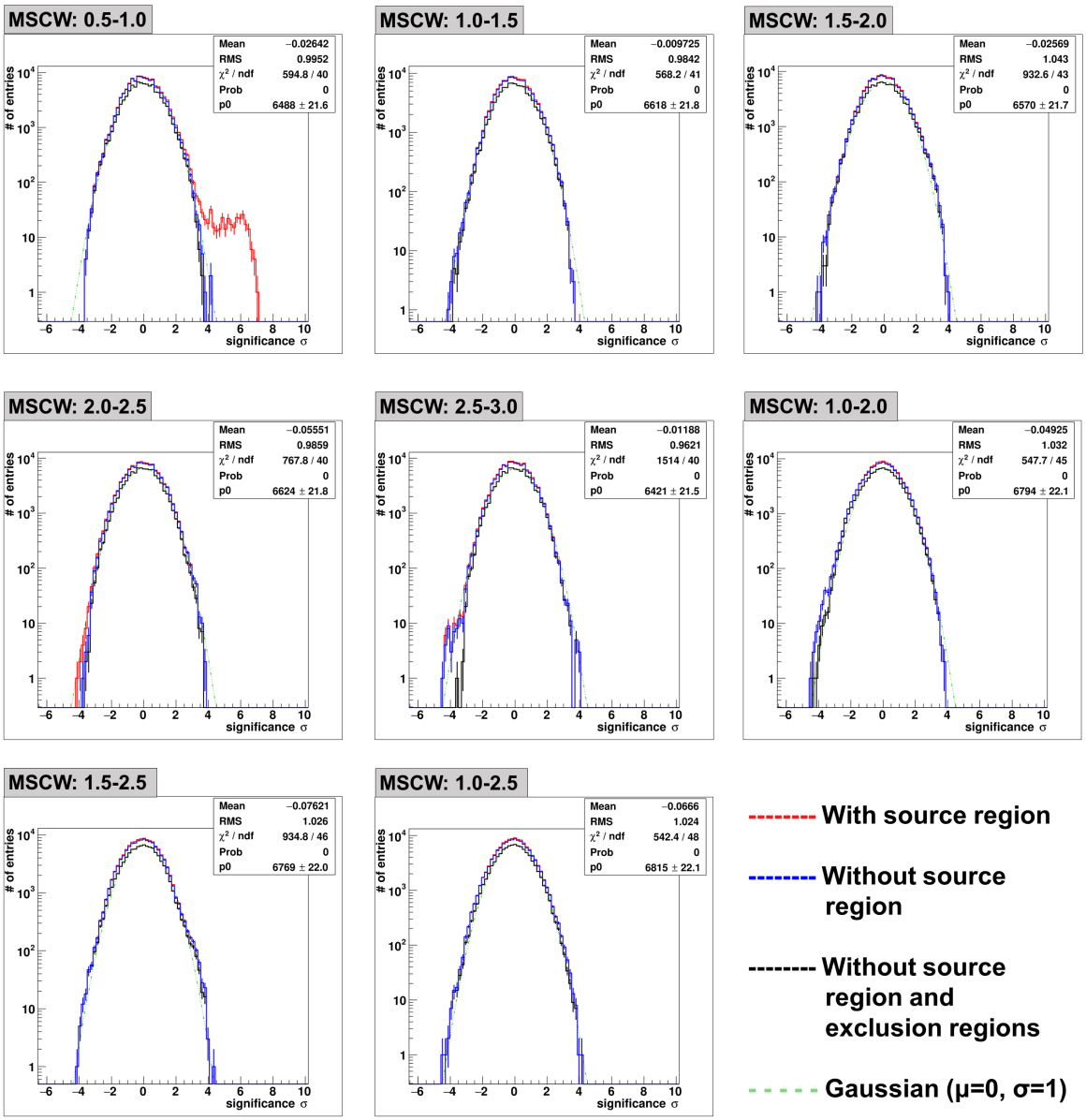

Figure 4.2: Significance distributions from a 4-hour exposure of the Crab Nebula. The exposure was analyzed with 8 potential MSCW regions for hadron counting.

Counts Per MSCW Range								
Run #	0.5-1.0	1.0-1.5	1.5-2.0	2.0-2.5	2.5-3.0	1.0-2.0	1.0-2.5	1.5-2.5
65311	240.0	263.0	293.0	246.5	198.5	556.0	803.0	540.0
65777	233.0	273.5	285.5	240.5	194.0	559.5	800.0	526.0
65778	229.0	247.0	296.0	250.5	187.0	543.5	794.5	547.0
65779	196.5	238.0	244.0	216.0	184.0	482.5	698.5	460.5
66003	170.5	201.5	218.5	197.0	151.0	420.0	617.0	415.5
66112	200.5	243.5	256.0	252.5	207.0	499.5	752.5	508.5
66113	220.0	249.0	254.5	252.5	204.5	503.5	756.0	507.0
66556	186.5	216.5	221.0	192.5	184.0	437.5	630.5	413.5
μ	209.50	241.50	258.56	231.00	188.75	500.25	731.44	489.75
σ	24.71	23.34	30.62	25.35	17.64	52.36	74.94	53.38
$\sqrt{N}$	14.47	15.54	16.08	15.20	13.74	22.37	27.05	22.13
σ_{rel}	11.79	9.67	11.84	10.97	9.34	10.47	10.25	10.90
ϵ_{rel}	6.91	6.43	6.22	6.58	7.28	4.47	3.70	4.52

Table 4.1: Statistics from analyzing a 4-hour exposure of the Crab Nebula. The exposure was analyzed for hadron counting: first, with 5 equally-sized potential MSCW ranges, then with 3 potential combined bins.

4.2 Consistency Analysis

I visualized the consistency and β distribution for 64 Segue 1 runs with 4032 possible OFF/ON combinations ($64^2 - 64 = 4032$).

All of the data that were classified as consistent were close to the line $\beta = 1$. For Δ_{Azimuth} and $\Delta_{\text{Elevation}}$, the frequency of both inconsistent and consistent data steadily decreased as the deviation increased (see Figure 4.3 and Figure 4.4). However, as Δ_{MJD} increased, the amount of inconsistent data increased, overtaking the amount of consistent data after about a year (see Figure 4.5). Elevation and azimuth are important observing parameters, but they do not intrinsically effect how γ-rays or hadrons are counted. The sensitivity of the VERITAS telescopes naturally decreases over time, effecting count rates. The separation in observation date between two runs thus has the greatest impact on whether they will be classified as consistent or inconsistent. Informed by these plots, I implemented the following tolerances in the MRM algorithm:

- $\Delta_{\text{Elevation}}$: 50°
- Δ_{Azimuth}: 45°
- Δ_{MJD}: 365 days

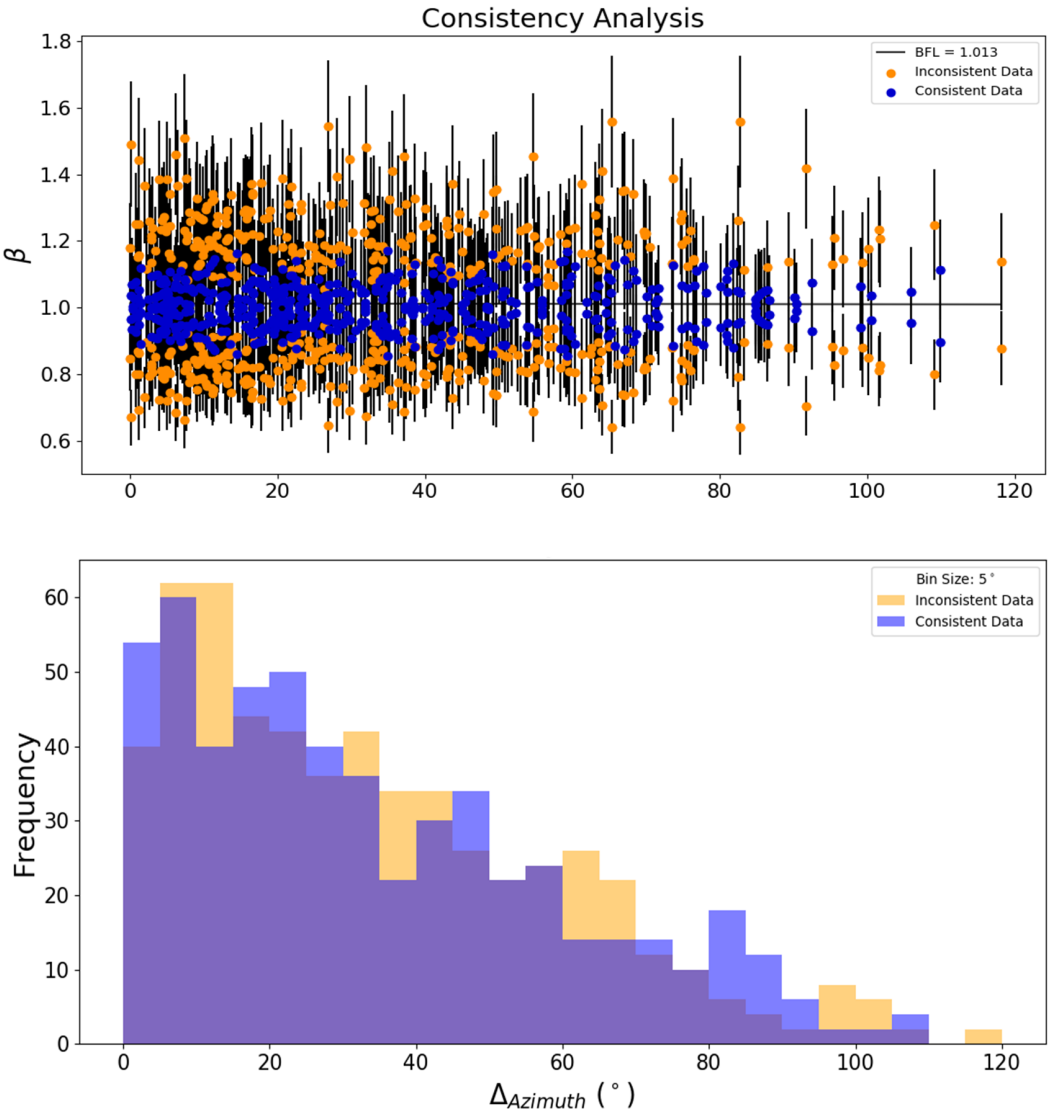

Figure 4.3: Consistency analysis for deviation in azimuth with 64 3-telescope runs of Segue 1.

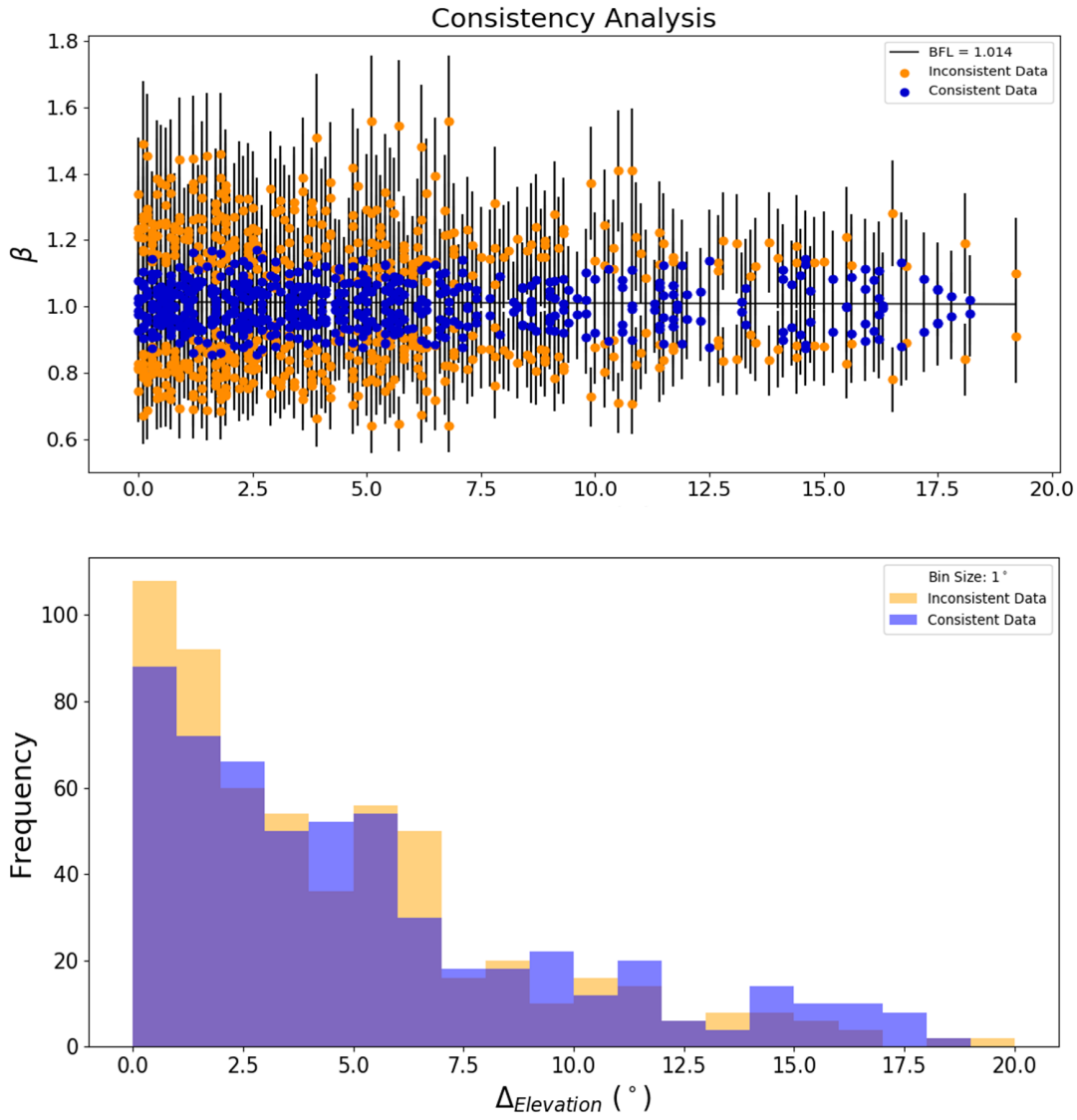

Figure 4.4: Consistency analysis for deviation in elevation with 64 3-telescope runs of Segue 1.

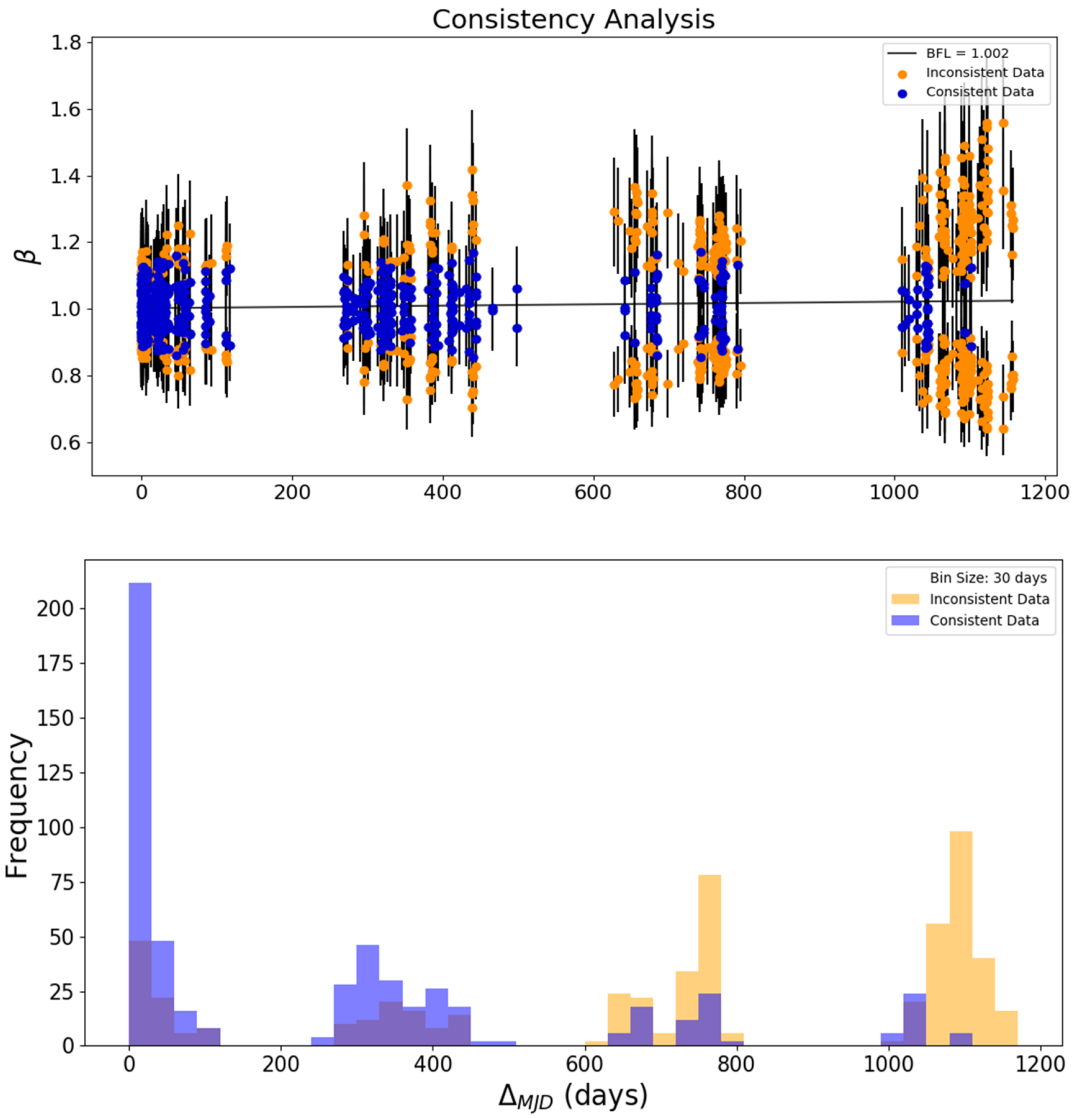

Figure 4.5: Consistency analysis for deviation in modified Julian date with 64 3-telescope runs of Segue 1.

4.3 MRM Analysis

The MRM algorithm that I optimized replicated the standard analysis results 4 times for 2 different sources. First, I analyzed 1ES 0229+200, a bright point source (see Figure 4.6 and Figure 4.7). Second, I analyzed Segue 1, a faint point source. Dwarf spheroidal galaxies are of interest to γ-ray astronomers searching for the predicted emission from dark matter particle decay. While I did not anticipate strong emission from Segue 1, I still selected this dim source to check for systematic uncertainties in the algorithm. Systematic uncertainties would get lost in the large number of 'measurements', or events, detected in bright sources like the Crab Nebula. As shown in Figure 4.8 and Figure 4.9, the curves for the source region, background region, and the Gaussian lie more or less on top of each other. This indicates a low systematic uncertainty and affirms that any hot or cold spots in the skymaps for Segue 1 are due to random fluctuations, not errors in the algorithm. The final source that I analyzed, Markarian 421, did not replicate the standard analysis results. As a target of opportunity, Markarian 421 has shorter and sparser observational periods. The runlist I used contained a 3-hour exposure with only 6 runs, which increased the impact of eliminating unmatched runs from the analysis.

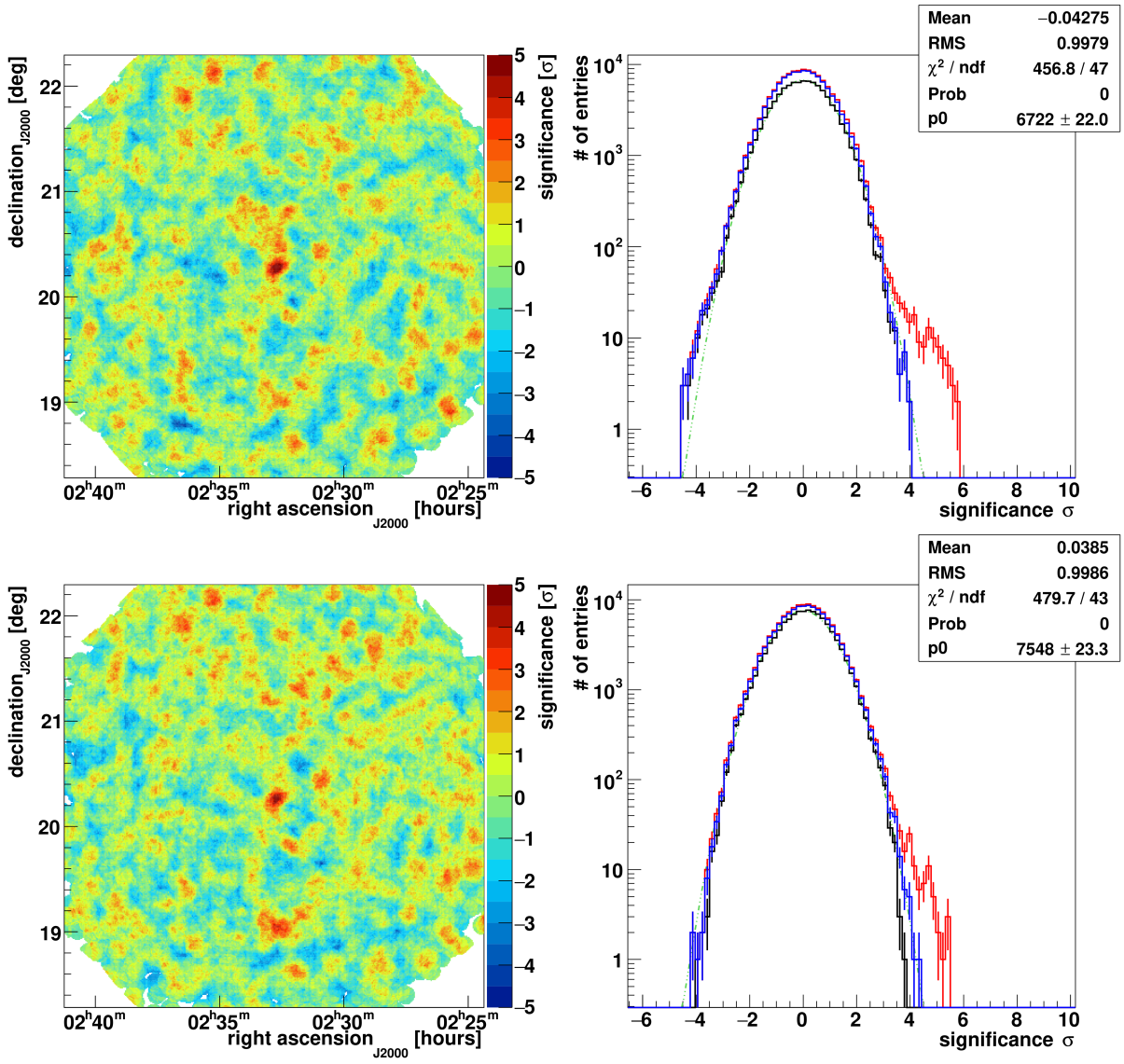

Figure 4.6: Skymap and significance distribution for hard, 3-telescope analysis of a 24.6-hour exposure of 1ES0229+200. *Top panels*: standard analysis; *bottom panels*: MRM analysis.

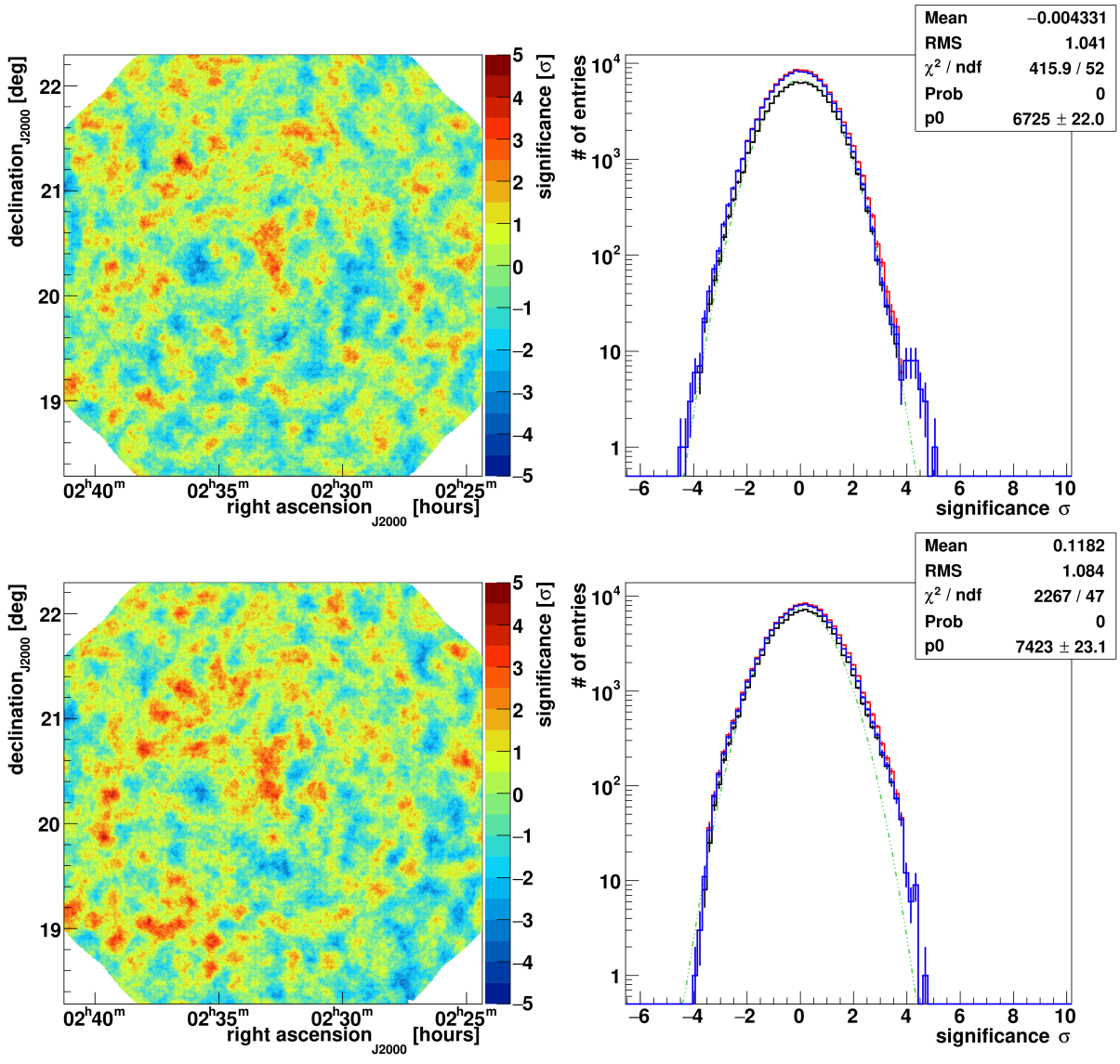

Figure 4.7: Skymap and significance distribution for moderate, 3-telescope analysis of a 23.1-hour exposure of 1ES0229+200. *Top panels*: standard analysis; *bottom panels*: MRM analysis.

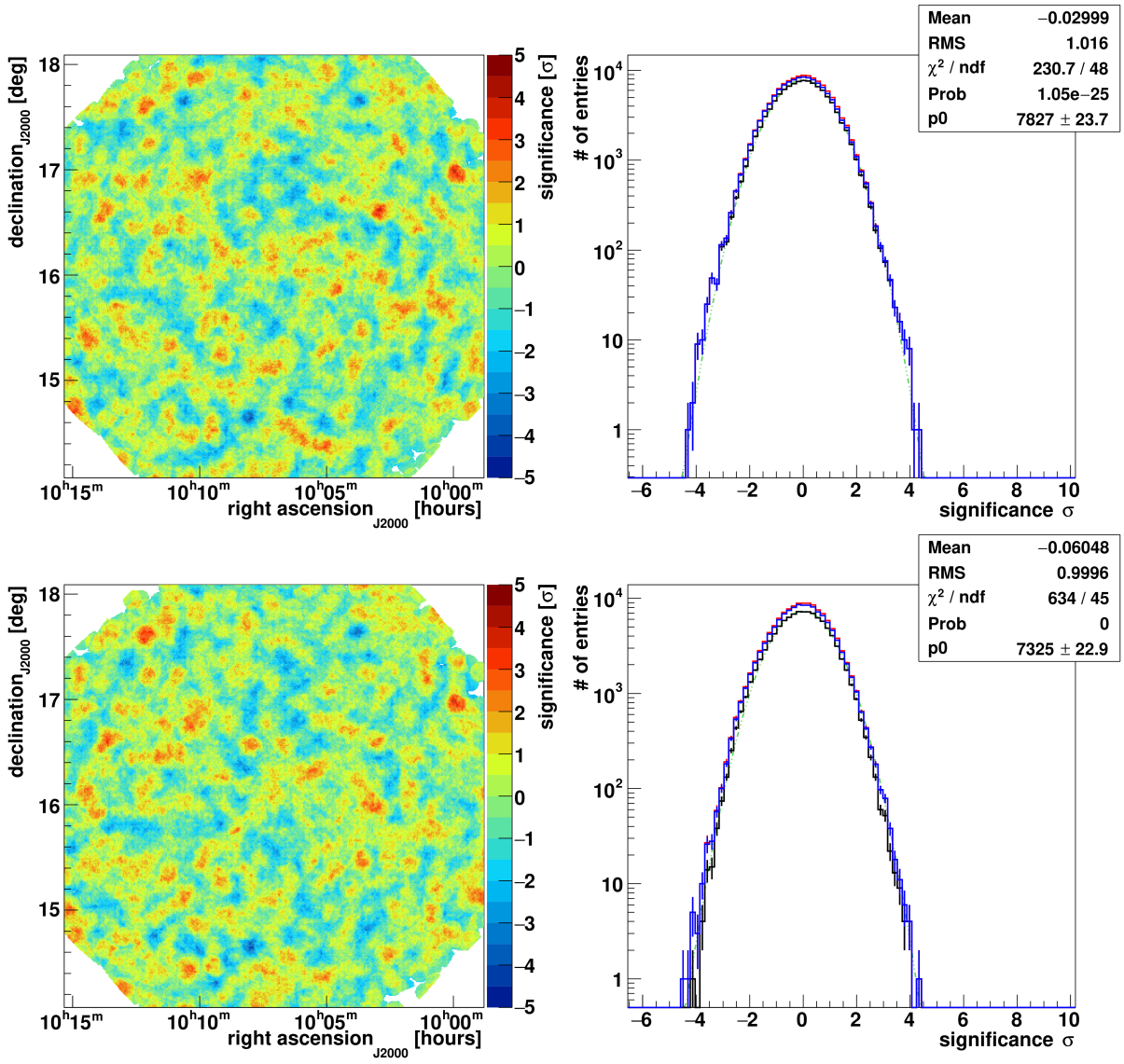

Figure 4.8: Skymap and significance distribution for hard, 3-telescope analysis of a 26.7-hour exposure of Segue 1. *Top panels*: standard analysis; *bottom panels*: MRM analysis.

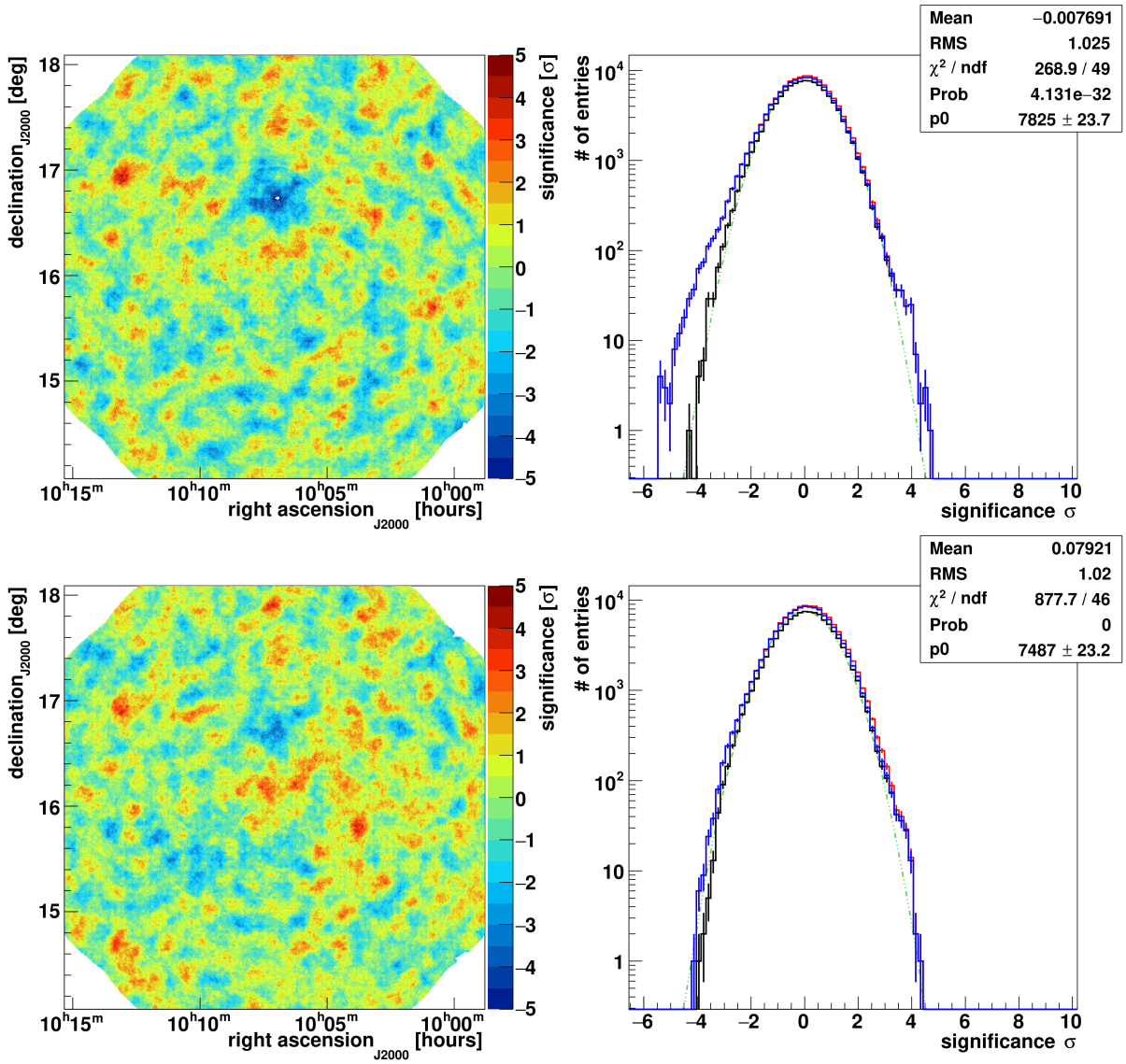

Figure 4.9: Skymap and significance distribution for moderate, 3-telescope analysis of a 23.9-hour exposure of Segue 1. *Top panels*: standard analysis; *bottom panels*: MRM analysis.

Chapter 5

CONCLUSIONS & FUTURE WORK

The MSCW range selected for γ-ray and hadron cuts has a significant effect on detection levels in skymaps and significance distributions. VERITAS users should attend to future telescope upgrades because they could necessitate modified calibration files in the EVENTDISPLAY pipeline.

The consistency analysis script predicted that MJD differences have the greatest impact on match success. This agrees with the expected wear and tear on the telescopes, as sensitivity will decline over time. Although implementing the MRM tolerances from simulated ON/OFF runlists still yielded significant results, it would be useful to modify the consistency analysis script. If it could take in an ON runlist from one source and an OFF runlist (of equal length) from 1+ sources, the MRM tolerances could be customized on a source-by-source basis. This would allow users to predict which OFF sources are the best to use for a given analysis.

The Segue 1 analysis demonstrated a low systematic uncertainty in the MRM algorithm. The algorithm has successfully replicated the standard analysis results from a dim source and a point source. Though if the VERITAS Collaboration is to accurately image Geminga, the MRM algorithm must be tested with more point sources (of varying brightness and peak energies) and extended sources. In addition, it would be favorable to modify the algorithm to work better with shorter runlists. Eliminating a few matched runs is negligible with a longer runlist, but for time-limited observations, this may present an issue.

Bibliography

[11] *ACT Techniques & VERITAS Technology*. 2011. URL: www.veritas.sao.arizona.edu/about-veritas-mainmenu-81/atmospheric-cherenkov-technique-and-veritas-technologies-mainmenu-87.

[Abd+09] A. A. Abdo et al. "Milagro Observations of Multi-TeV Emission from Galactic Sources in the Fermi Bright Source List". In: 700.2 (Aug. 2009), pp. L127–L131. DOI: 10.1088/0004-637X/700/2/L127. arXiv: 0904.1018 [astro-ph.HE].

[Abe+17] A. U. Abeysekara et al. "The 2HWC HAWC Observatory Gamma-Ray Catalog". In: 843.1, 40 (July 2017), p. 40. DOI: 10.3847/1538-4357/aa7556. arXiv: 1702.02992 [astro-ph.HE].

[BFH07] D. Berge, S. Funk, and J. Hinton. "Background modelling in very-high-energy γ-ray astronomy". In: 466.3 (May 2007), pp. 1219–1229. DOI: 10.1051/0004-6361:20066674. arXiv: astro-ph/0610959 [astro-ph].

[Di 19] Giuseppe Di Sciascio. "Ground-based Gamma-Ray Astronomy: an Introduction". In: *Journal of Physics Conference Series*. Vol. 1263. Journal of Physics Conference Series. June 2019, p. 012003. DOI: 10.1088/1742-6596/1263/1/012003. arXiv: 1904.06218 [astro-ph.IM].

[Fli15] Andy Flinders. "VERITAS Observations of the Geminga Supernova Remnant". In: *arXiv e-prints*, arXiv:1509.04224 (Sept. 2015), arXiv:1509.04224. arXiv: 1509.04224 [astro-ph.HE].

[Fun15] S. Funk. "Ground- and Space-Based Gamma-Ray Astronomy". In: *Annual Review of Nuclear and Particle Science* 65 (Oct. 2015), pp. 245–277. DOI: 10.1146/annurev-nucl-102014-022036. arXiv: 1508.05190 [astro-ph.HE].

[GC93] Neil Gehrels and Wan Chen. "The Geminga supernova as a possible cause of the local interstellar bubble". In: 361.6414 (Feb. 1993), pp. 706–707. DOI: 10.1038/361706a0.

[HH92] J. P. Halpern and S. S. Holt. "Discovery of soft X-ray pulsations from the γ-ray source Geminga". In: 357.6375 (May 1992), pp. 222–224. DOI: 10.1038/357222a0.

[Hil85] A. M. Hillas. "Cerenkov Light Images of EAS Produced by Primary Gamma Rays and by Nuclei". In: *19th International Cosmic Ray Conference (ICRC19), Volume 3*. Vol. 3. International Cosmic Ray Conference. Aug. 1985, p. 445.

[Hol+06] J. Holder et al. "The first VERITAS telescope". In: *Astroparticle Physics* 25.6 (July 2006), pp. 391–401. DOI: 10.1016/j.astropartphys.2006.04.002. arXiv: astro-ph/0604119 [astro-ph].

[MH17] Gernot Maier and Jamie Holder. *Eventdisplay: An Analysis and Reconstruction Package for Ground-based Gamma-ray Astronomy*. 2017. arXiv: 1708.04048 [astro-ph.IM].

[MS98] I. V. Moskalenko and A. W. Strong. "Production and Propagation of Cosmic-Ray Positrons and Electrons". In: 493.2 (Jan. 1998), pp. 694–707. DOI: 10.1086/305152. arXiv: astro-ph/9710124 [astro-ph].

[Wee03] T.C. Weekes. *Very High Energy Gamma-Ray Astronomy*. Cornwall: Institute of Physics Publishing, 2003.

[Wei08] A. Weinstein. "The VERITAS Trigger System". In: *International Cosmic Ray Conference*. Vol. 3. International Cosmic Ray Conference. Jan. 2008, pp. 1539–1542. arXiv: 0709.4438 [astro-ph].